ACS OMEGA

http://pubs.acs.org/journal/acsodf

Article

Thermally Activated Microstructural Evolution of PtIrCu Alloyed Nanorings: Insights from Molecular Dynamics Simulations

Tie-Jun Li, Wei-Hua Yang, Jin-Yan Pan,* Rao Huang, Gui-Fang Shao, and Yu-Hua Wen*

Cite This: *ACS Omega* 2022, 7, 37436−37441

Read Online

ACCESS | Metrics & More | Article Recommendations | Supporting Information

ABSTRACT: Nanoalloys have attracted extensive interest from the research and industrial community due to their unique properties. In this work, the thermally activated microstructural evolution and resultant collapse of PtIrCu nanorings were investigated using molecular dynamics simulations. Three PtIrCu nanorings with a fixed outer radius and varied inner radii were addressed to investigate the size effects on their thermal and shape stabilities. The shape factor was introduced to monitor their shape changes, and a common neighbor analysis was employed to characterize the local structures of atoms. The results reveal that both the thermal and shape stabilities of these nanorings can be remarkably improved by decreasing the inner radius. Furthermore, they all experienced the evolutionary process from ring to pie and spherelike morphologies, finally resulting in structural collapse. The stacking faults were observed in these rings during the heating process. Our work sheds light on the fundamental understanding of alloyed nanorings subjected to heating, hence offering a theoretical foundation for their syntheses and applications.

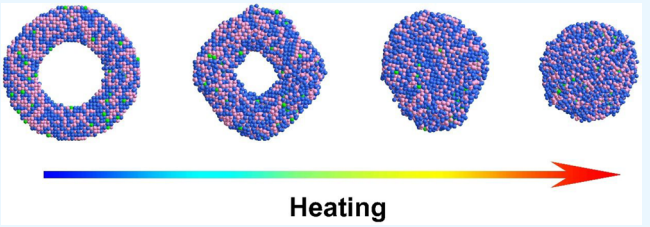

1. INTRODUCTION

Nanostructures have attracted great attention from both the academic and industrial areas over the past few decades due to their properties, which are different from those conventional materials. As of today, they have been used in many fields such as catalysis,[1−3] environmental protection,[4,5] and biomedicine.[6,7] It has been widely established that the crystal structure, composition, shape, and atomic distribution of nanoalloys dictate their properties and functions.[8−10] Notably, an effective way to realize a specific functionality is to synthesize alloyed nanostructures with well-defined shapes.[11] Thanks to the continuous development of synthetic techniques, the morphologies of nanostructures synthesized experimentally are diverse, ranging from nanospheres[12] to nanopolyhedrons,[13] nanorods,[14] nanorings,[15] and nanoframes.[16]

Among the nanostructures, metallic nanorings have attracted increasing attention in the past decade because of their excellent optical, magnetic, and catalytic properties.[17−19] To date, there have been reports regarding their syntheses and properties. For example, Liu et al. employed a scalable colloidal template technology based on a rotary coating platform to fabricate periodically concentric and eccentric metallic nanorings and nanocrescents with tunable structures.[20] Aizpurua et al. have found that Au nanorings, prepared by colloidal lithography, exhibit tunable plasmonic resonances in the near-infrared region.[17] Hu et al. have synthesized colloidal Au nanorings by using a galvanic replacement reaction and have found that the wavelength range of the local surface plasmonic resonance (LSPR) can be changed from 651 to 760 nm when their aspect ratios (the outer diameter-to-shell thickness ratios) increase from 3.8 to 7.1.[21] Ozel et al. used a new method based on coaxial lithography to prepare Au, Ag, Pt, Ni, and Pd nanorings and investigated the effects of the inner radius on the LSPR.[22] Especially, PtCu alloyed nanorings with a highly open hollow structure have been recently demonstrated to possess high catalytic activity and enhanced durability for the methanol oxidation reaction by doping with trace Ir to form $Pt_{0.75}Ir_{0.05}Cu$ alloy, suggesting that the properties of alloyed nanorings may be remarkably tuned by the introduction of appropriate elements.[23]

It is well-known that the thermal stability of nanoalloys is of great importance for their syntheses and practical applications.[24] Therefore, in this work we will direct our attention to the thermostability of PtIrCu alloyed nanorings. Taking $Pt_{0.75}Ir_{0.05}Cu$ nanoring as an example, we have constructed three nanorings with a fixed outer radius but varying inner radii and investigated the size effects on the thermal stability by using molecular dynamics simulations. Meanwhile, monometallic Pt and Cu nanorings have also been examined for comparison. This article is organized as follows. In section 2, the details of the models and calculations are described. The structural and shape evolutions of PtIrCu alloyed nanorings

Received: July 5, 2022
Accepted: October 6, 2022
Published: October 14, 2022

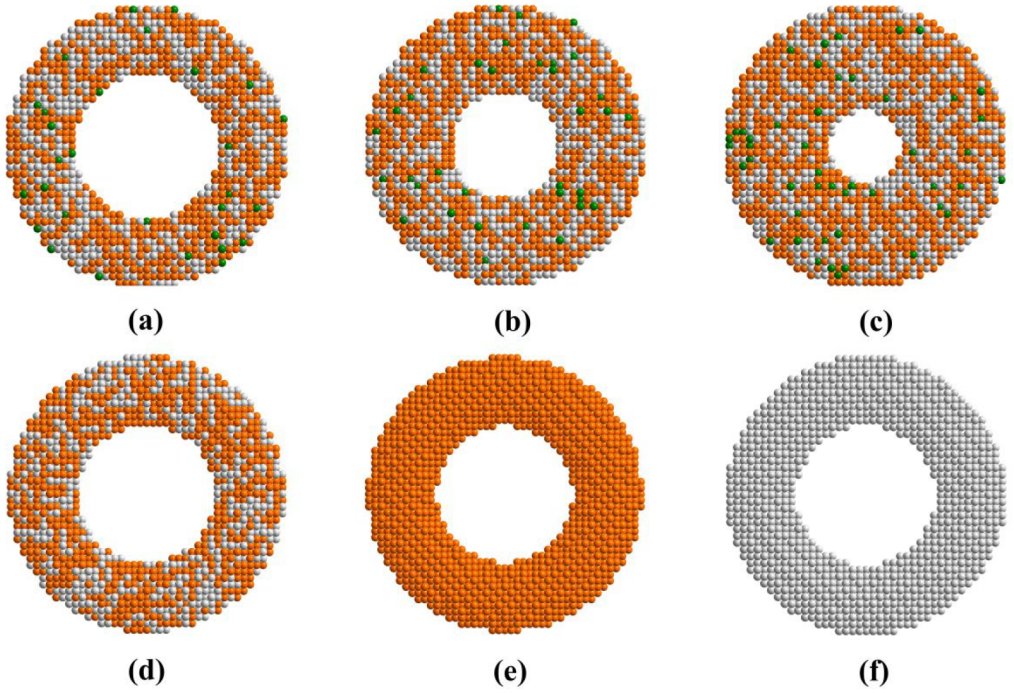

Figure 1. Schematic illustration of six nanorings: $Pt_{0.75}Ir_{0.05}Cu$ nanorings with inner radii of (a) R_1, (b) R_2, and (c) R_3; (d) $Pt_{0.75}Cu$, (e) Cu, and (f) Pt nanorings with an inner radius of R_1. The color denotes the type of atom: gray, Pt atom; orange, Cu atom; green, Ir atom.

during heating are discussed in section 3. The main conclusions are summarized in section 4.

2. COMPUTATIONAL METHODOLOGY

Six nanorings were constructed from a large bulk *fcc* crystal, as shown in Figure 1. Note that, in alloyed nanorings, atoms of metal elements are distributed randomly within the *fcc* lattice. Three $Pt_{0.75}Ir_{0.05}Cu$ alloyed nanorings with a fixed outer radius and varying inner radii were addressed so as to investigate the influence of the inner radius on the thermal stability of the nanorings (see Figure 1a–c). For the three nanorings, the outer radii are all set at 40 Å, and the inner radii R_1, R_2, and R_3 are 20, 15, and 10 Å, respectively. Correspondingly, the numbers of atoms are 4128, 5912, and 7636 in the nanorings, respectively. To investigate the effect of the introduction of Ir on the thermostability of alloyed nanorings, both $Pt_{0.75}Cu$ and $Pt_{0.75}Ir_{0.05}Cu$ nanorings were created with the same size (see Figure 1a,d). In addition, Pt and Cu nanorings were also constructed for comparison (see Figure 1e,f).

In molecular dynamics simulations, the Gupta potentials were used to describe the interaction of the atoms in the nanorings. They are based on the second-moment approximation of the tight-binding scheme (SMATB) and have been applied in many studies.[25−27] They include repulsive terms between atoms and many-body attraction terms. The formula for the total energy of a system composed of N atoms is expressed as

$$E = \sum_{i=1}^{N}\left\{\sum_{j=1,j\neq i}^{N} A\exp\left(-p\left(\frac{r_{ij}}{r_0}-1\right)\right) - \left[\sum\nolimits_{j=1,j\neq i}^{N}\xi^2\exp\left(-2q\left(\frac{r_{ij}}{r_0}-1\right)\right)\right]^{1/2}\right\} \quad (1)$$

where r_{ij} is the distance between atom i and atom j. The parameter r_0 represents the nearest-neighbor distance of atoms. The parameters A, P, ξ, and q were determined by fitting the bulk properties of the element, such as the cohesive energy, lattice parameter, and elastic constants. For alloys, the potential parameters can be obtained by using the geometric mean and arithmetic mean of the corresponding values for the single elements.[28] The potential parameters of Gupta potential used in this work are given in Table S1.

Prior to heating, the conjugate gradient method was used to minimize the total energy of the nanorings. Afterward, they were continuously heated by using molecular dynamics simulations under the NPT ensemble, in which the pressure, temperature, and number of atoms in the system were kept unchanged. The systems were heated from 0 to 1800 K with a temperature increment of 20 K. The relaxation time of each temperature was 250 ps, and in the last 20 ps, the physical quantities such as the potential energy, atomic coordinates, and velocities were extracted from the simulations. The Verlet velocity algorithm with a time step of 2 fs was used to integrate the equations of atomic motion in all the simulations. The Nose−Hoover thermal bath[29] and the Berendsen pressure "bath"[30] were respectively used to keep the nanorings at the expected temperature and pressure.

3. RESULTS AND DISCUSSION

The caloric curve is often used, both experimentally and theoretically, to monitor the phase transitions and identify the critical temperature for these transitions.[31−33] An abrupt increase in the potential energy and the corresponding peak

https://doi.org/10.1021/acsomega.2c04214
ACS Omega 2022, 7, 37436−37441

of heat capacity are generally regarded as a signal of a phase transition during heating. The temperature at which the maximum heat capacity is reached is taken as the melting point of the system. The formula of heat capacity can be written as[34]

$$C_p(T) = \frac{dE}{dT} + \frac{3}{2}R_{gc} \quad (2)$$

where E is the potential energy and R_{gc} = 8.314 J/(mol K).

Figure 2 shows the potential energy and heat capacity of three $Pt_{0.75}Ir_{0.05}Cu$ nanorings with different inner radii with

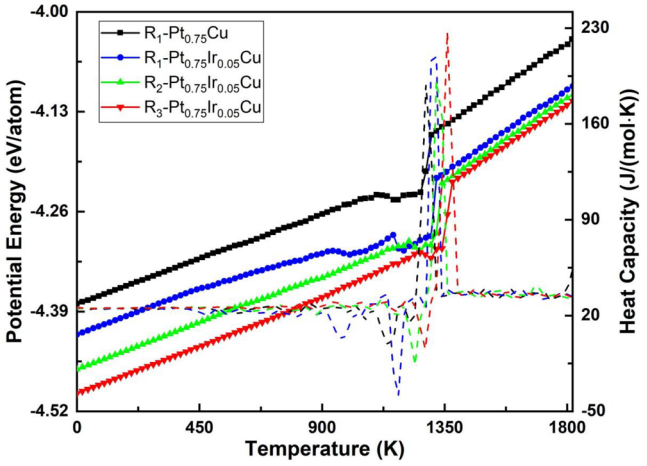

Figure 2. Temperature-dependent potential energies (solid lines) and corresponding heat capacities (dashed lines) of alloyed nanorings.

heating. The melting points of these nanorings are 1320, 1340, and 1380 K, respectively. In addition, the melting points of Pt, Cu, and $Pt_{0.75}Cu$ nanorings are 1400, 1160, and 1300 K, respectively (see Figure S1 and Figure 2 for their caloric curves). Generally, the structural stability of a material is determined by its energy at the ground state (i.e., its potential energy at 0 K), while its thermostability is evaluated by the overall melting temperature (i.e., the temperature where the maximum heat capacity occurs). By comparing the potential energy curves of $Pt_{0.75}Cu$ and $Pt_{0.75}Ir_{0.05}Cu$ nanorings with the same size, one can find that the energy of the latter is markedly lower than that of the former, indicating that the structural stability of the latter is superior to that of the former. Furthermore, the melting points also show that the latter has higher thermal stability than the former. These results suggest that the addition of Ir can improve both the structural and thermal stabilities of a PtCu alloyed nanoring. In addition, with an increase in temperature from 1160 to 1180 K, the potential energy of the $Pt_{0.75}Ir_{0.05}Cu$ nanoring with an inner radius of R_1 decreases, while this decrease is not apparent in the other two $Pt_{0.75}Ir_{0.05}Cu$ nanorings. The reason for the decreasing potential energy should be associated with the structural changes of these nanorings, which will be further discussed later.

In order to visualize the morphological evolution of the system during the heating process, the atomistic snapshots of the $Pt_{0.75}Ir_{0.05}Cu$ nanoring with an inner radius of R_1 at representative temperatures are illustrated in Figure 3. It can be seen from Figure 3a that there is no obvious deformation in the nanoring at room temperature. When the temperature is increased from 1160 to 1180 K, the pore in the nanoring gradually disappears (see Figure 3b,c), and the nanoring presents a pielike structure. Moreover, this pielike structure is maintained within a temperature range of 140 K or so. When the temperature reaches 1320 K, the nanoring further evolves from a pielike morphology into spherelike morphology. For the other two $Pt_{0.75}Ir_{0.05}Cu$ nanorings, the pielike structures form at 1240 and 1280 K, respectively (see Figure S2 for details), remarkably higher than that for the $Pt_{0.75}Ir_{0.05}Cu$ nanoring with R_1.

To investigate the structural evolution of the alloyed nanorings, the bond order parameter (BOP) was introduced to measure the aggregation or segregation behaviors of the constituent elements in alloys. It has also been widely used in the characterization of bimetallic nanoparticles.[35,36] The BOP of PtIrCu ternary alloy can be expressed as

$$\mathrm{BOP} = \frac{N_{Pt-Pt} + N_{Ir-Ir} + N_{Cu-Cu} - N_{Pt-Ir} - N_{Pt-Cu} - N_{Ir-Cu}}{N_{Pt-Pt} + N_{Ir-Ir} + N_{Cu-Cu} + N_{Pt-Ir} + N_{Pt-Cu} + N_{Ir-Cu}} \quad (3)$$

where N_{i-j} represents the number of bonds formed between atom types i and j. In general, the value of BOP falls within a region between 1 and −1. A positive value indicates clustering or phase separation in binary alloys, and a negative value signifies strong A−B bonding and chemical ordering. Note that the BOP value is 1 for a unary alloy, while it is zero for a completely disordered solid-solution binary alloy.

As an example, the calculated numbers of atomic bonds in the $Pt_{0.75}Ir_{0.05}Cu$ nanoring with R_1 at different temperatures are illustrated in Figure S3, displaying slightly increasing numbers in Pt−Pt, Pt−Cu, and Cu−Cu bonds during the melting. This indicates that changes in chemical ordering occur in the nanoring. Since the mole ratio of Pt, Ir, and Cu in $Pt_{0.75}Ir_{0.05}Cu$ alloy is 15:1:20, the ideal ratios of atomic bonds with different bonding types in chemically disordered alloy should be

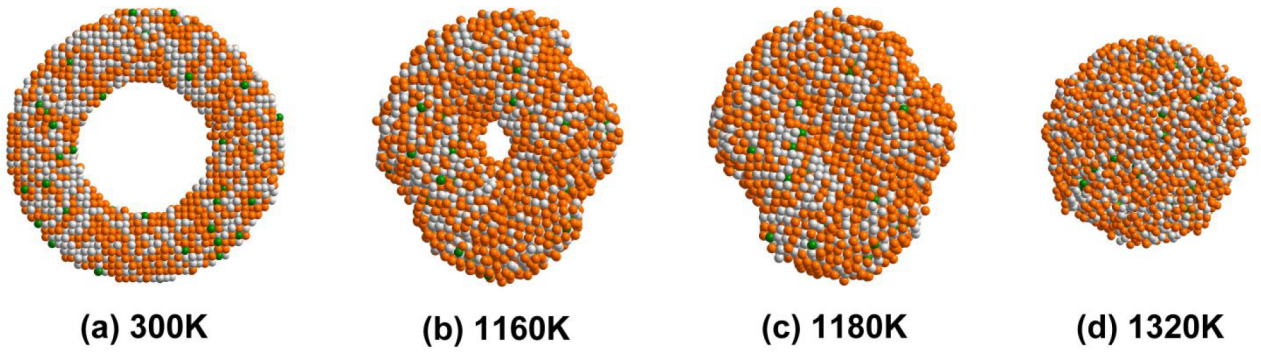

Figure 3. Snapshots of $Pt_{0.75}Ir_{0.05}Cu$ nanorings with R_1 at four representative temperatures.

https://doi.org/10.1021/acsomega.2c04214
ACS Omega 2022, 7, 37436−37441

$N_{Pt-Pt}:N_{Ir-Ir}:N_{Cu-Cu}:N_{Pt-Ir}:N_{Pt-Cu}:N_{Ir-Cu}$ = 225:1:400:30:600:40.

According to the numbers of atomic bonds, the BOP value of a uniform $Pt_{0.75}Ir_{0.05}Cu$ alloy should be −0.034. At the ground state, the BOP values of three $Pt_{0.75}Ir_{0.05}Cu$ alloyed nanorings are −0.027, −0.031 and −0.024, respectively, as shown in Figure 4. The three values above are close to −0.034,

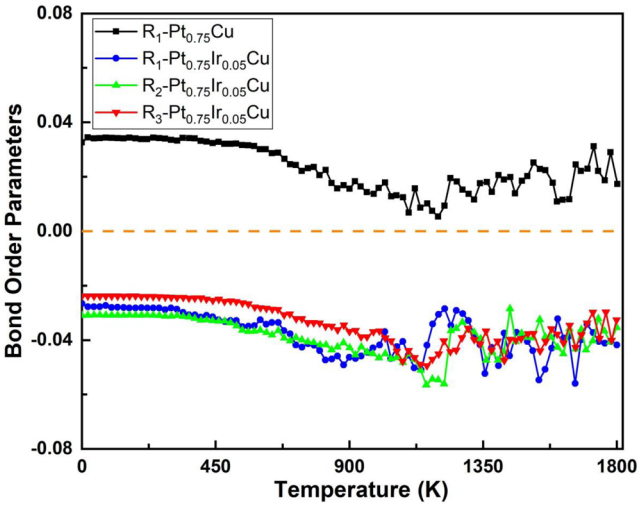

Figure 4. Temperature-dependent bond order parameters of alloyed nanorings with different inner radii.

which suggests that the atoms in the initial structures are uniformly distributed. As can be seen from Figure 4, the BOPs of the three nanorings tend to continuously decrease with temperature in the low-temperature region (typically below 1100 K) and fluctuate at high temperatures. Undoubtedly, this behavior should be closely associated with a dynamic distribution of atoms contributed by the enhanced diffusivity with increasing temperature. The BOPs of the nanoring gradually deviating from their initial values means that the distribution of atoms with different elements deviates somewhat from the uniformity. The gradually decreasing BOP before melting suggests that the nanorings tend to be chemically ordered. The BOP of the $Pt_{0.75}Cu$ nanoring also shows the same trend as those of the $Pt_{0.75}Ir_{0.05}Cu$ nanorings, but the difference is that the BOP of the former is always greater than zero.

As was discussed above, both the morphologies and structures of PtIrCu alloyed nanorings exhibit significant changes during the heating process. To further ascertain the critical temperature for the morphological change, we introduced the shape factor[37] to characterize the shape feature of the nanoring. It is defined as

$$s = \frac{1}{R^2}\sqrt{\frac{1}{N}\sum_{i=1}^{N}(r_i^2 - R^2)^2} \quad (4)$$

$$R = \sqrt{\frac{1}{N}\sum_{i=1}^{N} r_i^2} \quad (5)$$

where N represents the number of atoms in the nanoring and r_i is the distance from the ith atom to the particle center of mass.

Figure 5 illustrates the shape factors of six nanorings as a function of temperature. It can be seen that one of the

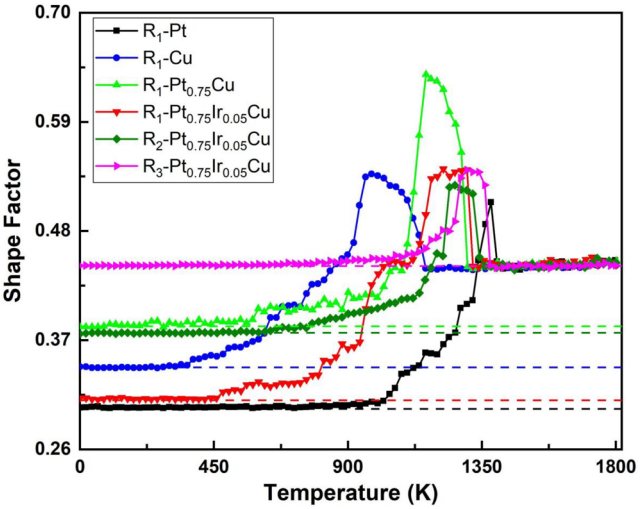

Figure 5. Temperature-dependent shape factors of six nanorings. The dashed lines correspond to the values at 0 K.

common features of these nanorings is that their shape factors basically remain constant at low temperatures, indicating that their initial shapes are well retained. In addition, the width of the low-temperature range can be used as a criterion to determine the shape stability of the nanorings to a certain extent. The temperature widths of Pt, $Pt_{0.75}Cu$, and Cu nanorings are 960, 560, and 360 K, respectively. Evidently, the temperature width of the $Pt_{0.75}Cu$ nanoring is between those of Pt and Cu nanorings, consistent with our expectation. The temperature widths of $Pt_{0.75}Ir_{0.05}Cu$ nanorings with the inner radii of R_1, R_2 and R_3 are 460, 640, and 820 K, respectively, indicating that the shape stability of $Pt_{0.75}Ir_{0.05}Cu$ nanorings is improved with decreasing inner radius. With a further increase of temperature, the shape factors of these nanorings present significant fluctuations before melting, meaning that their shapes are continuously changing. At 1380 K, all of the shape factors converge to 0.444, which is close to the ideal value of a sphere (0.435). This indicates that the shapes of all the nanorings are approximately spherelike after melting.

According to the aforementioned results, the initial shapes of all the nanorings could be well maintained at temperatures higher than room temperature (300 K), and the critical temperature for thermodynamic change is composition dependent. Among all the six nanorings, the Pt nanoring is the most stable while the Cu nanoring exhibits the worst stability. For direct methanol fuel cells (DMFCs), either a methanol oxidation reaction (MOR) at the anode or an oxygen reduction reaction (ORR) at the cathode usually proceeds at room temperature or a temperature slightly higher than 300 K.[23] Therefore, these nanorings as catalysts for fuel cells are able to retain their morphologies under the working conditions.

The common neighbor analysis (CNA), which provides a description of the local order of each atom by assigning different bonds to each pair of atoms that have common neighbors,[38] was employed to characterize the evolution of structural ordering in this work. All atoms in the nanoring are classified into four categories. Atoms in a local *fcc* order are considered to be "*fcc*" atoms. Atoms in a local *hcp* order are classified as "*hcp*" atoms, whose appearance in an *fcc* crystal is generally identified as the stacking fault. Atoms in icosahedral order are denoted as "*ico*" atoms, which are frequently found in

https://doi.org/10.1021/acsomega.2c04214
ACS Omega 2022, 7, 37436−37441

twinned particles such as Marks decahedral and icosahedral particles. The remaining atoms are categorized into "*other*" atoms.

Figure 6 illustrates the CNA results of the three PdIrCu nanorings. It can be seen that the ratio of structurally ordered

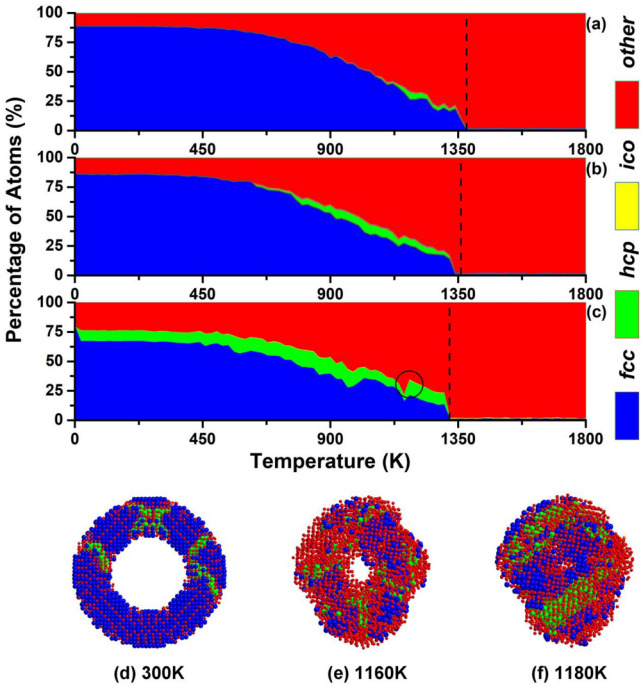

Figure 6. Temperature-dependent percentage of atoms with different structures in three $Pt_{0.75}Ir_{0.05}Cu$ nanorings with (a) R_3, (b) R_2, and (c) R_1. (d–f) Cross sections of snapshots of the $Pt_{0.75}Ir_{0.05}Cu$ nanoring with R_1 at three representative temperatures. Atoms are colored based on the CNA results.

atoms (including *fcc* and *hcp* atoms) gradually decreases with increasing temperature. For PdIrCu nanorings with small inner radii, no *hcp* atoms can be observed at low temperatures (see Figure 6a,b). However, Figure 6c shows that *hcp* atoms appear in the PdIrCu nanoring with a large inner radius at a temperature of 20 K. At the same time, the proportion of *fcc* atoms decreases, and the proportion of *other* atoms remains unchanged. This indicates that these *hcp* atoms have evolved from *fcc* atoms. In general, these *hcp* atoms tend to gather on the {111} plane to form stacking fault structures (see Figure 6d). According to the theory of crystal dislocations,[39] the formation of stacking faults is related to the nucleation and propagation of Shockley partial dislocation in an *fcc* crystal. It is worth mentioning that the formation of stacking faults in the $Pt_{0.75}Ir_{0.05}Cu$ nanoring with an inner radius of R_1 at remarkably low temperatures should be attributed to the existence of large pores, which is beneficial to the nucleation and activity of partial dislocations. As the temperature is increased further, the fractions of *fcc* and *hcp* atoms mostly decrease and the fraction of *other* atoms increases accordingly. When the temperature increases from 1160 to 1180 K, the fraction of *hcp* atoms in the $Pt_{0.75}Ir_{0.05}Cu$ nanoring increases from 4.8 to 12.6% and the fraction of *other* atoms decreases by 13% (see Figure 6c). The increase of *hcp* atoms in the range between 1160 and 1180 K exactly corresponds to the structural collapse of a $Pt_{0.75}Ir_{0.05}Cu$ nanoring into pielike structures without pores (see Figure 6c,f). Note that this phenomenon is inappreciable in the other two $Pt_{0.75}Ir_{0.05}Cu$ nanorings due to the small inner radius.

4. CONCLUSIONS

In summary, molecular dynamics simulations were used to investigate the thermostability and structural evolution of $Pt_{0.75}Ir_{0.05}Cu$ alloyed nanorings subjected to heating. Our results reveal that both the thermal and shape stability of these nanorings can be remarkably improved with decreasing inner radius. Furthermore, a comparison of $Pt_{0.75}Cu$ and $Pt_{0.75}Ir_{0.05}Cu$ nanorings demonstrates that the addition of Ir can improve the stability of a PtCu alloyed nanoring. The stacking faults tend to be formed in the PtIrCu nanorings with a large inner radius at relatively low temperatures. In the heating process, these nanorings undergo a continuously evolutionary process from ring to pie and then sphere, resulting finally in structural collapse. Our work suggests that the thermal and shape stability of alloyed nanorings can be tuned by introducing an appropriate element as well as controlling their inner radii. This study provides insights into the structure and stability of multimetallic nanorings, motivating the further design and synthesis of high-performance nanostructures.

■ ASSOCIATED CONTENT

Supporting Information

The Supporting Information is available free of charge at https://pubs.acs.org/doi/10.1021/acsomega.2c04214.

Potential parameters, potential energies, and atomistic snapshots of nanorings (PDF)

■ AUTHOR INFORMATION

Corresponding Authors

Jin-Yan Pan − *School of Ocean Information Engineering, Jimei University, Xiamen 361021, People's Republic of China*; Email: jypan@jmu.edu.cn

Yu-Hua Wen − *Department of Physics, Xiamen University, Xiamen 361005, People's Republic of China*; orcid.org/0000-0002-0578-7506; Email: yhwen@xmu.edu.cn

Authors

Tie-Jun Li − *School of Ocean Information Engineering, Jimei University, Xiamen 361021, People's Republic of China*

Wei-Hua Yang − *Department of Physics, Xiamen University, Xiamen 361005, People's Republic of China*

Rao Huang − *Department of Physics, Xiamen University, Xiamen 361005, People's Republic of China*; orcid.org/0000-0001-9913-2123

Gui-Fang Shao − *Department of Automation, Xiamen University, Xiamen 361005, People's Republic of China*; orcid.org/0000-0001-6189-2207

Complete contact information is available at: https://pubs.acs.org/10.1021/acsomega.2c04214

Notes

The authors declare no competing financial interest.

■ ACKNOWLEDGMENTS

This work was supported by the Natural Science Foundation of Fujian Province, China (Grant Nos. 2020J01714 and 2022J02001) and the Fundamental Research Funds for the Central Universities of China (Grant No. 20720220028).

REFERENCES

(1) Zhou, Z. Y.; Tian, N.; Li, J. T.; Broadwell, I.; Sun, S. G. Nanomaterials of high surface energy with exceptional properties in catalysis and energy storage. *Chem. Soc. Rev.* **2011**, *40*, 4167−4185.

(2) Zaera, F. Nanostructured materials for applications in heterogeneous catalysis. *Chem. Soc. Rev.* **2013**, *42*, 2746−2762.

(3) Fang, H.; Yang, J. H.; Wen, M.; Wu, Q. S. Nanoalloy Materials for Chemical Catalysis. *Adv. Mater.* **2018**, *30*, 1705698.

(4) Yu, X. L.; Shavel, A.; An, X. Q.; Luo, Z. S.; Ibáñez, M.; Cabot, A. Cu_2ZnSnS_4-Pt and Cu_2ZnSnS_4-Au Heterostructured Nanoparticles for Photocatalytic Water Splitting and Pollutant Degradation. *J. Am. Chem. Soc.* **2014**, *136*, 9236−9239.

(5) Lata, S.; Samadder, S. R. Removal of arsenic from water using nano adsorbents and challenges: A review. *J. Environ. Manage.* **2016**, *166*, 387−406.

(6) Verma, A.; Stellacci, F. Effect of Surface Properties on Nanoparticle-Cell Interactions. *Small* **2010**, *6*, 12−21.

(7) Wang, Y.; Zhao, Q. F.; Han, N.; Bai, L.; Li, J.; Liu, J.; Che, E. X.; Hu, L.; Zhang, Q.; Jiang, T. Y.; Wang, S. L. Mesoporous Silica Nanoparticles in Drug Delivery and Biomedical Applications. *Nanomedicine* **2015**, *11*, 313−327.

(8) Zhang, S.; Guo, S. J.; Zhu, H. Y.; Su, D.; Sun, S. H. Structure-Induced Enhancement in Electrooxidation of Trimetallic FePtAu Nanoparticles. *J. Am. Chem. Soc.* **2012**, *134*, 5060−5063.

(9) Huang, S. C.; Zhang, Y. S.; Zhang, X. L.; Wang, Z. G.; Yang, X. Y.; Zeng, Z. Mechanical Properties of Zirconium-Based Random Alloys: Alloying Elements and Composition Dependencies. *Comput. Mater. Sci.* **2017**, *127*, 60−66.

(10) Arno, M. C.; Inam, M.; Weems, A. C.; Li, Z. H.; Binch, A. L. A.; Platt, C. I.; Richardson, S. M.; Hoyland, J. A.; Dove, A. P.; O'Reilly, R. K. Exploiting the role of nanoparticle shape in enhancing hydrogel adhesive and mechanical properties. *Nat. Commun.* **2020**, *11*, 1420.

(11) Tao, A. R.; Habas, S.; Yang, P. D. Shape control of colloidal metal nanocrystals. *Small* **2008**, *4*, 310−325.

(12) Li, W. Q.; Hu, Z. Y.; Zhang, Z. W.; Wei, P.; Zhang, J. A.; Pu, Z. H.; Zhu, J. W.; He, D. P.; Mu, S. C.; Van Tendeloo, G. Nano-Single Crystal Coalesced PtCu Nanospheres as Robust Bifunctional Catalyst for Hydrogen Evolution and Oxygen Reduction Reactions. *J. Catal.* **2019**, *375*, 164−170.

(13) Sulaiman, J. E.; Zhu, S. Q.; Xiang, Z. L.; Chang, Q. W.; Shao, M. H. Pt-Ni Octahedra as Electrocatalysts for the Ethanol Electro-Oxidation Reaction. *ACS Catal.* **2017**, *7*, 5134−5141.

(14) Chen, Y. S.; Frey, W.; Kim, S.; Kruizinga, P.; Homan, K.; Emelianov, S. Silica-Coated Gold Nanorods as Photoacoustic Signal Nanoamplifiers. *Nano Lett.* **2011**, *11*, 348−354.

(15) Jang, H. Y.; Jang, H. J.; Park, D. K.; Yun, W. S.; Park, S. Fabrication of Shape-Controlled Reduced Graphene Oxide Nanorings by Au@Pt Nanoring Lithography. *Nanoscale* **2015**, *7*, 460−464.

(16) Chen, C.; Kang, Y. J.; Huo, Z. Y.; Zhu, Z. W.; Huang, W. Y.; Xin, H. L. L.; Snyder, J. D.; Li, D. G.; Herron, J. A.; Mavrikakis, M.; Chi, M. F.; More, K. L.; Li, Y. D.; Markovic, N. M.; Somorjai, G. A.; Yang, P. D.; Stamenkovic, V. R. Highly Crystalline Multimetallic Nanoframes with Three-Dimensional Electrocatalytic Surfaces. *Science* **2014**, *343*, 1339−1343.

(17) Aizpurua, J.; Hanarp, P.; Sutherland, D. S.; Käll, M.; Bryant, G. W.; de Abajo, F. J. G. Optical Properties of Gold Nanorings. *Phys. Rev. Lett.* **2003**, *90*, 057401.

(18) Lu, Y.; Shi, C.; Hu, M. J.; Xu, Y. J.; Yu, L.; Wen, L. P.; Zhao, Y.; Xu, W. P.; Yu, S. H. Magnetic Alloy Nanorings Loaded with Gold Nanoparticles: Synthesis and Applications as Multimodal Imaging Contrast Agents. *Adv. Funct. Mater.* **2010**, *20*, 3701−3706.

(19) Li, S. S.; Lv, J. J.; Teng, L. N.; Wang, A. J.; Chen, J. R.; Feng, J. J. Facile Synthesis of PdPt@Pt Nanorings Supported on Reduced Graphene Oxide with Enhanced Electrocatalytic Properties. *ACS Appl. Mater. Interfaces* **2014**, *6*, 10549−10555.

(20) Liu, X. F.; Choi, B.; Gozubenli, N.; Jiang, P. Periodic Arrays of Metal Nanorings and Nanocrescents Fabricated by a Scalable Colloidal Templating Approach. *J. Colloid Interface Sci.* **2013**, *409*, 52−58.

(21) Hu, Y.; Chou, T. M.; Wang, H. J.; Du, H. Monodisperse Colloidal Gold Nanorings: Synthesis and Utility for Surface-Enhanced Raman Scattering. *J. Phys. Chem. C* **2014**, *118*, 16011−16018.

(22) Ozel, T.; Ashley, M. J.; Bourret, G. R.; Ross, M. B.; Schatz, G. C.; Mirkin, C. A. Solution-Dispersible Metal Nanorings with Deliberately Controllable Compositions and Architectural Parameters for Tunable Plasmonic Response. *Nano Lett.* **2015**, *15*, 5273−5278.

(23) Shi, Y.; Fang, Y.; Zhang, G. L.; Wang, X. S.; Cui, P.; Wang, Q.; Wang, Y. X. Hollow PtCu Nanorings with High Performance for the Methanol Oxidation Reaction and Their Enhanced Durability by Using Trace Ir. *J. Mater. Chem. A* **2020**, *8*, 3795−3802.

(24) Ferrando, R.; Jellinek, J.; Johnston, R. L. Nanoalloys: From Theory to Applications of Alloy Clusters and Nanoparticles. *Chem. Rev.* **2008**, *108*, 845−910.

(25) Michaelian, K.; Rendon, N.; Garzon, I. L. Structure and Energetics of Ni, Ag, and Au Nanoclusters. *Phys. Rev. B* **1999**, *60*, 2000−2010.

(26) Schebarchov, D.; Baletto, F.; Wales, D. J. Structure, Thermodynamics, and Rearrangement Mechanisms in Gold Clusters-Insights from the Energy Landscapes Framework. *Nanoscale* **2018**, *10*, 2004−2016.

(27) Wen, Y. H.; Li, L.; Li, Y. M.; Huang, R. Structural Evolution of the Surface and Interface in Bimetallic High-Index Faceted Heterogeneous Nanoparticles. *J. Phys. Chem. Lett.* **2021**, *12*, 2454−2462.

(28) Wen, Y. H.; Li, L.; Zhao, T.; Huang, R. Solid−Liquid Coexistence in Trimetallic Heterostructured Nanoparticle Catalysts: Insights from Molecular Dynamics Simulations. *ACS Appl. Nano Mater.* **2020**, *3*, 12369−12378.

(29) Evans, D. J.; Holian, B. L. The Nose−Hoover Thermostat. *J. Chem. Phys.* **1985**, *83*, 4069−4074.

(30) Berendsen, H. J. C.; Postma, J. P. M.; van Gunsteren, W. F.; DiNola, A.; Haak, J. R. Molecular Dynamics with Coupling to an External Bath. *J. Chem. Phys.* **1984**, *81*, 3684−3690.

(31) Noya, E. G.; Doye, J. P. K.; Calvo, F. Theoretical Study of the Melting of Aluminum Clusters. *Phys. Rev. B* **2006**, *73*, 125407.

(32) Chirot, F.; Feiden, P.; Zamith, S.; Labastie, P.; L'Hermite, J. M. A Novel Experimental Method for the Measurement of the Caloric Curves of Clusters. *J. Chem. Phys.* **2008**, *129*, 164514.

(33) Hock, C.; Schmidt, M.; von Issendorff, B. Low-Temperature Caloric Behavior of a Free Sodium Nanoparticle. *Phys. Rev. B* **2011**, *84*, 113401.

(34) Qi, Y.; Cagin, T.; Johnson, W. L.; Goddard, W. A. Melting and Crystallization in Ni Nanoclusters: The Mesoscale Regime. *J. Chem. Phys.* **2001**, *115*, 385−394.

(35) Aguilera-Granja, F.; Vega, A.; Rogan, J.; Andrade, X.; García, G. Theoretical Investigation of Free-Standing CoPd Nanoclusters as a Function of Cluster Size and Stoichiometry in the Pd-Rich Phase: Geometry, Chemical Order, Magnetism, and Metallic Behavior. *Phys. Rev. B* **2006**, *74*, 224405.

(36) Wen, Y. H.; Huang, R. Effect of Chemical Ordering on Thermal Stability of Pt−Co Nanoparticles. *J. Phys. Chem. C* **2019**, *123*, 12007−12014.

(37) Wang, Z. L.; Zhong, Y. Q.; Wang, S. Y. A New Shape Factor Measure for Characterizing the Cross-Section of Profiled Fiber. *Text. Res. J.* **2012**, *82*, 454−462.

(38) Honeycutt, J. D.; Andersen, H. C. Molecular Dynamics Study of Melting and Freezing of Small Lennard-Jones Clusters. *J. Phys. Chem.* **1987**, *91*, 4950−4963.

(39) Schiøtz, J.; Vegge, T.; Tolla, F. D. D.; Jacobsen, K. W. Atomic-Scale Simulations of the Mechanical Deformation of Nanocrystalline Metals. *Phys. Rev. B* **1999**, *60*, 11971−11983.

https://doi.org/10.1021/acsomega.2c04214
ACS Omega 2022, 7, 37436−37441